A graphene-edge ferroelectric molecular switch

José M. Caridad[1*], Gaetano Calogero[1], Paolo Pedrinazzi[1,2], Jaime E. Santos[1,3], Anthony Impellizzeri[1,4], Tue Gunst[1], Timothy J. Booth[1], Roman Sordan[2], Peter Bøggild[1*], Mads Brandbyge[1*]

[1]*Centre for Nanostructured Graphene (CNG), Department of Micro- and Nanotechnology, Technical University of Denmark, 2800 Kongens Lyngby, Denmark*

[2]*L-NESS Laboratory, Department of Physics, Politecnico di Milano, 20133 Milano, Italy*

[3] *Centro de Física and Departamento de Física, Universidade do Minho, P-4710-057 Braga, Portugal*

[4]*Dipartimento di Fisica e Astronomia, Università di Catania, Via Santa Sofia, 95125 Catania, Italy*

[*]corresponding authors: jcar@ dtu.dk, peter.boggild@ dtu.dk, mads.brandbyge@ dtu.dk

We show that polar molecules (water, ammonia and nitrogen dioxide) adsorbed solely at the exposed edges of an encapsulated graphene sheet exhibit ferroelectricity, collectively orienting and switching reproducibly between two available states in response to an external electric field. This ferroelectric molecular switching introduces drastic modifications to the graphene bulk conductivity and produces a large and ambipolar charge bistability in micron-size graphene devices. This system comprises an experimental realization of envisioned memory capacitive (memcapacitive) devices whose capacitance is a function of their charging history, here conceived via confined and correlated polar molecules at the one-dimensional (1D) edge of a two-dimensional (2D) crystal.

Keywords: graphene, graphene edges, polar molecules, memcapacitor, ferroelectricity, hysteresis

Molecular switches comprise a new range of solid-state electronic systems able to reversibly shift molecules between two or more states[1,2]. In recent years, several switches based on single-molecules have been created on solid surfaces implementing simple functionalities such as transistors or photoconductors[1,2]. The development of more advanced architectures and electronic capabilities at a molecular level requires, however, the understanding and control of collective interactions between molecules composing these systems[3]. Such scenario may be created in molecules possessing long-range dipolar interactions confined to surfaces of reduced dimensionality[4], enabling the generation of strongly correlated, ferroelectric systems with a switchable response. In the present work, we demonstrate that these novel functionalities can be achieved by confining polar molecules at the edge of a graphene sheet. Specifically, we show large, ambipolar charge bistabilities in the electrical characteristics of encapsulated, gated graphene devices with oxygenated edges exposed to gas environments containing different polar molecules. It is important to note that this ambipolar behavior does not occur in two distinct cases: *(i)* when the polar gas surrounding the oxygenated edges of graphene devices is replaced by a non-polar gas and *(ii)* when the edges of the encapsulated devices are fluorinated, regardless whether the environment contains polar gasses or not. Both of these observations clearly point out that graphene edges and polar molecules are the key contributors to the observed phenomenon, indicating that polar molecules adsorbed at oxidized graphene edges become polarized, which we find affect the graphene bulk conductivity via capacitive coupling. In other words, the aforementioned observations cannot be ascribed to other device components such as the hBN and SiO_2 dielectrics or the metal contacts.

We provide a simplified atomistic model of the system based on Density Functional Theory (DFT) calculations, which is able to capture the alignment of a single chain of polar molecules adsorbed at edges of gated graphene devices with oxygen termination. Combining these results with a phenomenological device model, we are able to reproduce our experiments in qualitative and quantitative terms. This overall ferroelectric system comprises an experimental instance of newly envisioned memory capacitive (memcapacitive) devices[5,6], here undertaken at a molecular level and with promising perspectives in terms of developing efficient circuitry for artificial neural computing[6,7].

Experimental results and discussion

The adsorption of molecular species on graphene has been extensively studied as an efficient approach to modify its electronic properties, and can result in both reversible insertion of charge carriers in the monolayer[8-10] and the permanent modification of its electronic band structure[11,12]. To

date, the focus has largely been on adsorption on the graphene basal plane, assuming a negligible contribution from edge adsorbed species. The behavior of molecules adsorbed exclusively at the graphene edge remains relatively unexplored despite their critical role in determining the physical and chemical properties of this 2D crystal.[13-16] Following published techniques for the exfoliation and van der Waals assembly of 2D materials[17-19], we have fabricated micrometer-size, encapsulated, graphene field-effect devices where only the graphene edges are exposed to the ambient environment in order to evaluate the adsorption of polar molecules at these locations (Figures 1(a) and (b)). Importantly, we note that edges of these graphene devices are exposed to fluorine- and oxygen based plasma treatments during and after fabrication, a fact which induces their fluorination or oxidation, respectively (details in Methods).

Figure 1(c) shows the measured resistance $R = V/I$ of one of our devices (Device 1) treated with oxygen plasma as a function of the gate-voltage V_g under three different environmental conditions: vacuum (<10^{-3} mbar, red), dry air (blue) and dry air mixed with 1% water vapour (black). In each of these cases, we have performed two gate-voltage sweeps in opposite directions, either starting from a positive or negative maximum gate-voltage $V_g^{\max}$. Results for each of the three environmental conditions are shown with the negative sweep direction $+V_g^{\max} \rightarrow -V_g^{\max}$ as continuous lines and the positive sweep direction $-V_g^{\max} \rightarrow +V_g^{\max}$ as dashed-dotted lines. For both the vacuum and dry air curves the resistance $R(V_g)$ is independent of the sweep direction, with a charge neutrality point V_{CNP} located at -4 V ($V_{CNP}{}^0$) due to residual dopants near the graphene layer[17-19].

Strikingly, the charge neutrality point in $R(V_g)$ under 1% water vapour is shifted symmetrically around $V_{CNP}{}^0$ by ΔV_{CNP} ~ +7 V or -7 V when starting the gate-sweep from $+V_g^{\max}$ or $-V_g^{\max}$, respectively. In other words, our graphene device with oxygen plasma post-treated edges exhibits large, symmetric and switchable episodes of homogeneous *p*- or *n*- doping depending on the respective starting point of the sweep sequence. This hysteretic doping behavior is almost completely quenched (ΔV_{CNP} ~ 0.5V) in the same encapsulated device after the fluorine-based plasma treatment, as shown in Figure 1(d). The residual ΔV_{CNP} of 0.5V can be accounted for by imperfect fluorine functionalization of the graphene edges[20].

The observation of symmetrical gate voltage history dependent doping of oxygen-treated graphene edges in the presence of water vapour indicates that the interaction between the polar water and the

oxidized graphene edge are responsible for the observed charge bistability, while other parts of the device, such as the hBN and SiO_2 dielectrics or the metal contacts, are not. Additional reasoning regarding why this charge bistability phenomenon cannot be accounted for by commonly reported hysteretic effects in literature are described in Supporting information, Note 1.

We have confirmed the appearance of this phenomenon in multiple encapsulated devices with oxidized graphene edges and water molecules (Figure 2 and Supporting information, Note 1). In addition, we have carried out three additional experiments in order to clarify the nature of this effect.

First, we show that ΔV_{CNP} increases by increasing the magnitude of the maximum gate voltage $V_g^{\max}$ in the sweep (Figure 2(a)). This observation shows that the applied gate voltage (or correspondingly, the electric field existing at graphene edges E_{loc} [21,22], see Supporting Information, Note 2) impacts the actual microscopic structure and alignment of the adsorbed water molecules at graphene edges, suggesting that a larger applied electric field results in a higher degree of molecular polarization of water at the edges.

Secondly, we observe that the initial application of a gate voltage (electric field) on the system from V_g = 0 V polarizes and aligns water molecules adsorbed at edges, as found from consecutive gate voltage sweeps $0 \rightarrow +V_g^{\max} \rightarrow 0$. Figure 2(b) shows that at t = 0, when sweeping V_g from $0 \rightarrow +V_g^{\max}$, the V_{CNP} of the device is close to V_g=0 V (corresponding to the value measured in vacuum V_{CNP}^0 for this device). When sweeping from $+V_g^{\max} \rightarrow 0$ the V_{CNP} of the device has shifted substantially to ~20 V. After waiting 30 s at V_g=0 V, we repeat the sweep $0 \rightarrow +V_g^{\max}$. The V_{CNP} of the device is seen to remain at V_g ~20 V (instead of returning to V_{CNP}^0), clearly indicating stable polarization of water at the graphene edge in response to the applied gate voltage.

Third, if polarization of edge-bound polar molecules is responsible for this effect, then polar molecules other than water should cause a similar behavior. To test this, we consecutively expose one device to three individual environments composed of one of the following polar substances: water vapour H_2O, ammonia NH_3 or nitrogen dioxide NO_2, at 1% in dry air. Prior to and between measurement in each of the three environments, the chamber was evacuated to $<10^{-3}$ mbar to avoid cross-contamination, and the return of the CNP to the original position of V_{CNP}^0 was confirmed. Figure 2(c) shows that exposure to these three different polar molecules all exhibit the same previously observed episodes of symmetric and ambipolar doping, although to different degrees. This strongly implies that the mechanism responsible of this phenomenon is general for polar molecules,

and effectively rules out exclusive interactions occurring within water molecules[23], oxygen-water or even carbon-water interactions as causing this effect. More importantly, this observation clearly implies Coulomb interactions between polar molecules or between polar molecules and the (chemistry-dependent) graphene edge potential[13] as the relevant microscopic causes of the observed two-state macroscopic polarization of polar molecules adsorbed at the oxidized edges of encapsulated graphene devices.

We note that ferroelectricity is predicted[24,25] and claimed[26] to occur in confined systems with ordered polar molecules as a result of enhanced dipolar interactions appearing in systems with reduced dimensionality[25,26]. Figure 2(b) shows how ΔV_{CNP} progressively increases for the NO_2, NH_3 and H_2O cases, respectively; a behavior that is readily explained as a direct consequence of the different dipole moment μ_d of these molecules: $\mu_d^{NO_2}$ (0.4D) $< \mu_d^{NH_3}$ (1.74D) $< \mu_d^{H_2O}$ (1.85D) (see Eq.1 and the analytical model proposed below).

The experimentally observed charge bistability is seen only for oxygen plasma treated graphene edges exposed to polar species. For ferroelectric ordering of polar edge molecules to cause a measurable change in the electrical response we require two conditions to be met: *(i)* a stable (but not necessarily complete) alignment of polar molecules as obtained upon application of an external electric field to the device, and *(ii)* interactions between the polar molecular ensemble and the chemistry-dependent graphene edge as well as intermolecular Coulomb interactions leading to macroscopical changes in the charge distribution.

Alignment of polar molecules at graphene edges

We use a simple atomistic model in order to understand the binding energy ε_b of polar molecules adsorbed at the edges of a finite-size graphene sheet for different edge passivation using Density Functional Theory (DFT) with an incorporated gate field (Methods). This model, Figure 3(a), incorporates the key elements of the experimental system, comprising the gating of a finite-size graphene sheet modelled here as a nanoribbon with oxidized or fluorinated edges and the presence of polar molecules in their proximity of these edges (see Methods). Complete details of the equilibrium positions and the calculation of the binding energies of all combinations of polar molecules (H_2O, NH_3, NO_2) and graphene terminations (oxygen, fluorine) considered in our experiments can be found in Supporting Information, Notes 3, 4. Numerical values for the binding energies of all the tested cases are presented in Table 1. In general, ε_b between 0.5-1 eV are obtained for all three polar molecules adsorbed at oxidized graphene edges, values close to the ones reported in literature[14,15]. Instead ε_b is more than 3 times smaller for the calculated case of H_2O adsorbed at a fluorinated

graphene edges. This behavior agrees with the fact that C-O bonds at the edges enhance the adsorption strength of polar molecules at those positions[14,15].

Table 1. Calculated binding energies of different molecules adsorbed at a graphene edges with different terminations.

Edge termination	***Polar molecule***	ε_b ***(eV)***
Oxygen (O)	Water (H_2O)	0.508
Oxygen (O)	Nitrogen dioxide (NO_2)	0.937
Oxygen (O)	Ammonia (NH_3)	0.534
Fluorine (F)	Water (H_2O)	0.159

Figure 3(b) shows that at $V_g = 0\ \mathrm{V}$, after relaxing the structure, the individual polar molecules are randomly trapped in one of only two allowed equilibrium positions. These positions are symmetrically oriented with respect to the graphene basal plane, a behavior that has already been reported in previous studies[15]. Importantly, this equally-probable, two-state trapping is broken for devices with oxygenated edges when $V_g \neq 0\ \mathrm{V}$ i.e., in the presence of the local electric field E_{loc} existing at the edge of finite-size devices[21,22]. We demonstrate this by calculating (Figure 3(c)) the total energy difference of the system ($\varepsilon_{\mathrm{tot}}^{(z<0)} - \varepsilon_{\mathrm{tot}}^{(z>0)}$) when the polar molecules are placed below $\varepsilon_{tot}^{(z<0)}$ and above $\varepsilon_{tot}^{(z>0)}$ the graphene plane $(z=0)$, for different averaged carrier densities in the device n_{avg} (or equivalently V_g or E_{loc}). The energy difference $\varepsilon_{\mathrm{tot}}^{(z<0)} - \varepsilon_{\mathrm{tot}}^{(z>0)}$ increases linearly with n_{avg} (or V_g , E_{loc}), crosses the origin and changes sign with n_{avg} (or V_g , E_{loc}). First, this behavior indicates that one of the two available configurations is favored for $V_g \neq 0\ \mathrm{V}$ for oxygenated graphene edges. Second, a larger fraction of the population of polar molecules are positioned in the more favorable configuration for larger n_{avg}, with the final occupation depending ultimately on the maximum value of carrier density reached $n_{avg}^{\max}$ (equivalently $E_{loc}^{\max}$ or $V_g^{\max}$). Finally, the more favorable position for an individual molecule flips upon changing the sign of n_{avg}, i.e. the system is ambipolar. These

behaviors are qualitatively identical irrespective of the studied polar species, but quantitative differences in $\varepsilon_{\text{tot}}^{(z<0)} - \varepsilon_{\text{tot}}^{(z>0)}$ between different molecules at any fixed n_{avg} are observed (i.e. different slopes), and are present even for full coverage (Figure 3(c), lower inset).

These simulations agree with our experimental trends. In particular, the favoring of one of two available positions for the polar molecules at graphene edges when $V_g \neq 0$ V is consistent with the observed bistable macroscopic charge states in our gated device. Furthermore, the population of these two molecular states in the system (i.e. molecular alignment) is indeed regulated by the external field E_{loc}, and depends quantitatively on the actual dipole moment of the polar molecule, as observed in experiments (Figures 2(a) and 2(c), respectively). Moreover, the preferential trapping in any of the two calculated possible configurations observed in devices with oxygenated edges does not exist in the case of fluorinated edges for any V_g. Figure 3(c, upper inset) clearly shows that the energy difference $\varepsilon_{\text{tot}}^{(z<0)} - \varepsilon_{\text{tot}}^{(z>0)}$ does not change with n_{avg} (V_g or E_{loc}) in devices with fluorine passivated edges. This indicates that in this case, the population of the two states is not controlled by an external field, in perfect agreement with the quenched charge bistability observed in our encapsulated graphene devices after a fluorine-based plasma treatment (Figure 1(d)).

Finally, we note that the DFT results are robust upon variations of the choice of functional (Methods), the width of our simulated graphene nanoribbon (Methods) and the edge chirality of the device: zigzag or armchair (Supporting information, Note 5). The latter fact provides a compelling reason for the charge bistability phenomenon being present in our experimental graphene devices, having edge roughness ~1 nm[22] and thus likely composed of a mixture of both edge chiralities. We also note that despite not accounting for temperature and pressure in our DFT calculations, we predict complete (1:1) edge coverage of polar molecules in our devices under the given experimental conditions by statistical mechanics calculations (Supporting Note 6). Such calculations explicitly account for the effect of molecular mobility (rotation, vibration) and the possible adsorption and desorption of polar species from graphene edges at the given temperature and pressure of the experiments.

Capacitive coupling of aligned polar molecules on the electrical characteristics of graphene devices

Collectively oriented and correlated polar molecules favoring either of the two observed states at graphene edges would generate a net dipole moment with a component perpendicular to the graphene plane p_z. We demonstrate below that p_z has a measurable effect on the electrical characteristics

$R(V_g, p_z)$ of a micron-size graphene device via capacitive coupling. Up to a first approximation, p_z will depend on[27]:

$$p_z = \mu_d N \eta, \qquad (1)$$

where μ_d is the dipole moment of a single polar molecule, N the total number of adsorbed polar molecules at the edges (corresponding in our case to the total number of available binding sites, see above and Supporting information Note 6), and $\eta = (N^{(z>0)} - N^{(z<0)})N^{-1}$, the relative difference in the number of molecules above ($N^{(Z>0)}$) and below ($N^{(Z<0)}$) the graphene plane with respect to the gate. Considering μ_d and N as fixed parameters for a given system, $-1<\eta<1$ determines its current state and consequent behavior.

The resistance R of a micrometer size, gated graphene transistor is inversely proportional to the total charge Q that exists in the monolayer[28] :

$$R \propto \frac{1}{\sqrt{Q^2 + Q_{res}{}^2}} \qquad (2)$$

where Q_{res} is a residual charge due to unwanted doping and/or thermally activated carriers[28]. In the present case, Q will depend on both the back gate-voltage V_g and the net dipole moment p_z along the edge of graphene $Q(V_g, p_z)$ and can be calculated electrostatically from the two contributions to the total surface charge density $\sigma = \sigma_B + \sigma_C$. Here, σ_B represents the bulk contribution (solely) due to the direct gate-induced carrier injection in the system. Meanwhile, σ_C is the additional contribution due to the oriented polar molecules, which have a notable effect close to the edges of the device. The detailed description of this electrostatic model appears in the Supporting information, Note 7. We note that σ_C and η are the only free parameters of this electrostatic model, and can be extracted from the experimental data. Moreover, σ_C depends on η, as we demonstrate below by a mean-field calculation reflecting the molecular switching mechanism. Therefore, η is the only independent parameter of the proposed phenomenological model.

Figure 4 (a) shows the calculated resistance of a micrometer-scale graphene device for three cases: absence of polar molecules ($p_z = 0$), and full edge occupancy of polar molecules all oriented in one

of the two possible orientations, (e.g. at $|\eta^{\max}|=1$ and $|p_z|=\mu_d N$). The experimentally observed ambipolar resistance $R(V_g, p_z)$ is clearly reproduced by the calculations.

Specifically, we took μ_d=1.85D as the dipole moment of water while *N* is estimated for full coverage as $N=4L/a_b$, where $4L$ is the perimeter of our device and a_b is the mean distance between binding sites at the graphene edge (given by the second nearest neighbor distance in a graphene lattice ~0.25 nm). With these assumptions, the separation ΔV_{CNP} between resistance curves agrees quantitatively with our experiments (Figure 1(c)) for a $\sigma_C{}^{\max}$ of 0.08 C/m^2 in this case. The evolution of σ_C (or equivalently η) with respect to V_g therefore describes the ferroelectricity of the system.

Molecular switching mechanism: mean-field model

We propose a ferroelectric model of molecular switching to simultaneously estimate both the fraction $\eta(V_g,T)$ of polarized molecules at a given V_g and temperature T (or equivalently the charge redistribution induced in our graphene device due to the presence of polar molecules $\sigma_C(V_g,T)$). The ferroelectric switching model for an ensemble of molecules is based on the observed charge bistability in our experiments and is inspired by the mean-field Curie-Weiss model of magnetism. Using Boltzmann statistics, at temperature T and for a given local electric field E_{loc} at the edge of the device generated by the back-gate, the probability of molecules being either above or below the graphene plane is:

$$N^{(z>0)}=e^{\Delta\varepsilon/k_BT},\quad N^{(z<0)}=e^{-\Delta\varepsilon/k_BT}, \quad (3)$$

where the energy $\Delta\varepsilon=E_{eff}\mu_d\equiv(K\eta+b)k_BT$ represents the energy to flip a single dipole μ_d in the effective electric field E_{eff} which exists at the edge for $V_g\neq 0$ and finite polarization. The term $b=E_{\mathrm{loc}}\mu_{\mathrm{d}}/(k_{\mathrm{B}}T)$ contains all the interactions to which a single dipole is subjected at an electric field E_{loc} (electric field for η=0 in the device). Meanwhile, $K\eta=\Delta E_{\mathrm{eff}}\mu_{\mathrm{d}}/(k_{\mathrm{B}}T)$ describes the response to the local field at the edge $\Delta E_{\mathrm{eff}}=E_{\mathrm{eff}}-E_{\mathrm{loc}}$ when $\eta\neq 0$. This effective interaction parameter *K* describes the redistribution of charge between the graphene edge and bulk due to the finite polarization, which, in turn, change the local field at the edge and provide a feedback mechanism between local field and polarization.

Given $\eta = (N^{(z>0)} - N^{(z<0)})N^{-1}$, our problem is reduced to solving numerically the transcendental equation $\eta = \tanh(K\eta + b)$ (Figure 4(b)). Using Eqs (1) and (2), $R(V_g, p_z)$ can be calculated; the results are shown in Figure 4(c).

Importantly, in this model K is the only free parameter (since ΔE_{eff} is related to $\sigma_C(r)$, Supporting Information Note 8) which describes the actual microscopic arrangement of the polar molecules, including, for instance, situations where more than one row of molecules are present at the graphene edge. Given the experimentally observed $|\Delta V_{CNP}|$, this mean-field model enables independent determination of K, the maximum polarization achieved in the system η^{max}, and the surface charge density ${\sigma_C}^{max}$ of the corresponding device (see Supporting Information, Note 8). For the specific case of our experimental device in Figure 1(c) with a $|\Delta V_{CNP}|$ ~ 7 V, these values are, $\eta^{max} \sim 0.84$, $K \sim 1.4$ and ${\sigma_C}^{max} \sim 0.03$ C/m^2. The values obtained for η^{max} and σ_C are consistent with those previously assumed (η^{max} = 1) and estimated (${\sigma_C}^{max}$ ~0.08 C/m^2) above from electrostatic calculations.

Consequently, K is the key parameter describing the observed ferroelectric behavior of polar molecules at graphene edges: ferroelectricity would not exist in the system for $K < 1$. At a microscopic level, K is a result of molecular dipole-graphene edge interactions as well as intricate intermolecular (dipole-dipole) interactions. We note that the effect of the screening interaction (charge distribution) has been predicted to lead to the alignment of the molecular dipoles normal to the bulk graphene basal plane, even at room temperature[29]. However, the screening and electrostatic potential is more complex at the edge where it depends e.g. on edge passivation[13]. The non-trivial interplay between the molecular adsorption at passivated graphene edges, graphene-molecule interactions and molecule-molecule interactions will determine the equilibrium configuration of polar molecules at graphene edges (see examples in Supporting information, Note 4) and the appearance of ferroelectricity.

Memcapacitive behavior

Using Eq. (2), the experimental device capacitance $C(V_g, p_z) = Q(V_g, p_z)/V_g$ is seen to be hysteretic, ambipolar and divergent (Figure 5). These are the three unique features of memory-capacitive systems[5,7]. This behavior arises at the molecular level as a result of the ferroelectricity of confined polar molecules at the graphene edges affecting the charge transport in the monolayer. The gate sweeps shown in Figure 2(b) in effect demonstrate the "write" and "read" operations for this

memcapacitive device. At t = 0, the V_{CNP} of the device is close to V_g=0 V (V_{CNP}^0) since the polar molecules trapped at graphene edges are randomly distributed in the two available states ($p_z = 0$). An increasing degree of polarization (corresponding to the "write" operation, grey line) occurs while increasing V_g, with the state of the system stored in the form of a change of the V_{CNP} to ~20 V, after returning to V_g=0 V. Even after 30 s at V_g=0 V, V_{CNP} is seen to remain at ~20 V when performing subsequent "read" operations (red sweep, $0 \rightarrow V_g^{\max}$), and thus the state of the memcapacitor is persistent at room temperature over unexpectedly long timescales given its molecular origin.

In summary, we have demonstrated that individual polar molecules at the edges of an encapsulated graphene device display a switchable and stable dipole alignment in response to an external electric field, leading to net dipole, which causes a pronounced macroscopic charge bistability in gated graphene devices**.** This molecular system represents an experimental instance of envisioned memcapacitive devices[5-7] and can be exploited for the exploration of correlated molecular systems[4,24-26] and applications such as neuromorphic hardware architectures[7].

Materials and methods

Device fabrication. The fabrication process[19] is based on the dry-pickup and encapsulation of graphene between hexagonal boron nitride (hBN)[17,18]. We select hBN flakes with thicknesses between 15 and 25 nm for our devices. Stacked hBN/graphene/hBN heterostructures are placed on top of a highly doped Si wafer with a 300 nm SiO_2 on top. Square devices are shaped from these heterostructures by electron beam lithography (EBL) and reactive ion etch (RIE) etching steps. The RIE process comprises an initial SF_6 etch (20 secs) for the top hBN (power ~30 W, 30 sccm), a brief oxygen-based plasma etch (10 secs) for graphene (power ~40 W, argon 40 sccm, oxygen 5 sccm) and by a second SF_6 etch (20 secs) for the bottom etch (power ~30 W, 30 sccm). We emphasize the usage of RIE etching as an effective way to reduce the edge disorder in graphene devices[22,30].

The contacting procedure[19] comprises a second EBL step performed to define the contacts of the device, followed by the evaporation of Cr/Pd/Au (2 nm, 15 nm and 25nm respectively) and a lift-off.

The definition of the device perimeter by etching leaves only the graphene edges exposed to the ambient environment. Here, the edge termination is essential in our devices. We expose the edge of graphene in our devices to both fluorine-based (SF_6) and oxygen (O) plasmas, in order to evaluate the adsorption of polar molecules with respect to the edge passivation of graphene. Fluorine decoration at

the edge is achieved by a plasma treatment at room temperature with SF_6 as precursor gas[20,31]. In other words, we have explicitly avoided the usage of CF_4 plasma due to its tendency to introduce excessive disorder in graphene[20]. Meanwhile, oxygen decoration at the edge is achieved by a short (1 sec) plasma ashing (power ~20 W) post-treatment, a gentle, chemical and undirected process[30].

In practice, graphene is subjected to a fluorine edge treatment while etching the bottom hBN with the fluorine-based plasma (SF_6), during the fabrication of hBN the encapsulated graphene devices. We note here that this explains why the effect is previously unreported for encapsulated devices[18]. Instead, oxygen decoration of graphene edges is achieved afterwards by annealing first devices up to 400 degrees Celsius in vacuum ($<10^{-5}$ mbar) for 2 hours to eliminate residual fluorine existent from the fabrication process[32]. Then, devices will be exposed to 1 sec of oxygen plasma to facilitate the complete oxidation of graphene edges[30]).

Electrical measurements. Our measurements were performed in a dark and environmentally controlled chamber. Measurements of resistance were performed using a Stanford SR830 lock-in amplifier with an excitation voltage of 200 μV at a frequency of 17.77 Hz. The gate-voltage sweeps were carried out at a rate of 0.2 V/s. We have confirmed the homogeneity[33] of our fabricated devices by comparing the measurement in the configuration shown in Figure 1(c), with a measurement carried out with the wiring configuration rotated by 90 degrees[17,33]. We measure first devices where the edge of graphene is treated with SF_6 as a result of the entire device fabrication (finished by etching the bottom hBN). Then, we measure devices after being subjected to the vacuum annealing and the 1s oxygen plasma ashing processes, steps undertaken to remove fluorine and promote a complete oxygenation of the graphene edges in the device.

Atomistic Simulations. Our density functional theory (DFT) calculations are performed with the software ATOMISTIX TOOLKIT. The wave functions are expanded in terms of a localized single zeta-polarized basis set and double zeta-polarized basis set. We use norm-conserving Troullier-Martins pseudopotentials with a density mesh cutoff of 75 Hartree, the LSDA exchange-correlation by Perdew and Zunger[34] and a 1x5x1 (6x6x1) k-point grid with origin at Γ for the ribbon calculations. We represent the direction perpendicular to the graphene plane as the *z* direction (Figure 3(a)). In order to assess the robustness of the results with respect to intermolecular interactions, we introduce 1, 2 or 4 polar molecules per unit cell. Due to periodic boundary conditions in the *y* direction, this corresponds to having an infinitely long edge with coverages 0.25, 0.5 and 1 of the bay sites[23]. We place polar molecules with the center of mass slightly out of the graphene plane and then relax the structure. Geometry optimization were performed until all forces were below 0.01 eV/ Å. Binding energies of all tested molecules adsorbed at the edge of graphene and equilibrium

configurations are shown in the Supporting information, Note 3. We note that the optimized configurations with both single and double zeta polarized basis sets are in good agreement with other DFT studies in literature at zero gate voltage [14,23].

To simulate finite electrostatic gating we add a charge to the graphene layer and solve the Poisson equation with Dirichlet (Neumann) boundary condition at the gate electrode (vacuum boundary)[35].

In our simplified model, the presence of the hBN dielectric and the possible presence of water molecules assembled at its edges is not explicitly accounted for, however, such effects would be included in the effective interaction parameter *K*. We do not expect dielectric screening effects to play a central role, as the experiments show that edge termination (O or F) is the main determinant for the amplitude of the hysteresis alongside the adsorbant dipole moment.

We calculate the total energy ε_{tot} of polar molecules adsorbed at the edge of a graphene nanoribbon passivated with fluorine or oxygen atoms, following experiments and hydrogen, a common reference element used to passivate graphene edges[23].

Although the simulated ribbon is much smaller than the experimental micron-size devices, the total energy difference $\varepsilon_{\mathrm{tot}}^{(z<0)} - \varepsilon_{\mathrm{tot}}^{(z>0)}$ is independent of the extent of the graphene basal plane[14]. We have checked this by simulating ribbons of different widths *W* (3 nm, 13 nm and 23 nm), obtaining very similar results in all these cases.

Furthermore, we have undertaken an appropriate electrostatic scaling by choosing the ribbon width and its distance to the gate electrode. This is clearly seen in the generated carrier densities in the device n_{avg} (Figure 3), having similar values than experiments. Thus, E_{loc} and the electrostatic energy of interaction $\mu_d E_{loc}$ (playing a role in ε_{tot}) are similar for simulated ribbons and experimental micron-size devices.

Finally, our DFT results show the same behavior for both zigzag and armchair termination of the graphene nanoribbon (Supporting Information Note 5), providing a compelling reason for a robust charge bistability phenomenon to be present in experimental graphene devices, even with borders composed of a mixture of both edge chiralities.

References

1. C. Jia, A. Migliore, N. Xin, S. Huang, J. Wang, Q. Yang, S. Wang, H. Chen, D. Wang, B. Feng, Z. Liu, G. Zhang, D-H. Qu, H. Tian, M.A. Raner, H.Q. Xu, A. Nitzan, X. Guo, Covalently bonded single-molecule junctions with stable and reversible photoswitched conductivity. *Science* **352** 1443 (2016)
2. J. Martínez-Blanco, C. Nacci, S.C. Erwin, K. Kanisawa, E. Locane, M. Thomas, F. vonn Oppen, P. W. Brouwer and S. Fölsh, Gating a single-molecule transistor with individual atoms. *Nat.Phys*. **11**, 640 (2015)
3. Y. Zhang, H. Kersell, R. Stefak, J. Echeverria, V. Iancu, U.G.E. Perera, Y. Li, A. Deshpande, K.-F. Braun, C. Joachim, G. Rapenne and S.-W. Hla, Simultaneous and coordinated rotational switching of all molecular rotors in a network. Nat. Nanotechnol. **11**, 706 (2016)
4. S. Sinha and L. Santos, Cold dipolar gases in quasi-one-dimensional geometries. Phys. Rev. Lett 99, 140406 (2007)
5. M. Krems, Y.V. Pershin and M. Di Ventra, Ionic Memcapacitive effects in Nanopores. *Nano Lett.* **10**, 2674 (2010)
6. J. Martinez-Rincon, M. Di Ventra and Y. Pershin, Solid-state memcapacitive system with negative and diverging capacitance. *Phys. Rev. B* **81**, 195430 (2010)
7. D. Tran and C. Teuscher, Memcapacitive Devices in Logic and Crossbar Applications. *IUJC*, **13**, 35 (2017)
8. F. Schendin, A.K. Geim, S.V. Morozov, E.W. Hill, P. Blake, M.I. Katsnelson and K.S. Novoselov, Detection of individual gas molecules adsorbed on graphene. *Nature Mat*. **6** 652 (2007)
9. P. Solís-Fernández, S. Okada, T. Sato, M. Tsuji, H. Ago, Gate-Tunable Dirac Point of Molecular Doped Graphene. *ACS Nano*, **10**, 2930 (2016)
10. T.O. Wehling, K.S. Novoselov, S.V. Mozorov, E.E. Vdovin, M.I. Katsnelson, A.K. Geim A.I. Lichetenstein, Molecular Doping of Graphene. *Nano Lett*. **8**,1 (2008)
11. C-H. Chang, X. Fan, L-J. Li and J-L. Kuo, Band gap tuning of graphene by adsorption of aromatic molecules. *J. Phys. Chem. C* **116**, 13788 (2012)
12. F. Yavari, C. Kritzinger, C. Gaire, L. Song, H. Gulapalli, T. Borca-Tasciuc, P.M. Ajayan and N. Koratkar, Tunable bandgap in graphene by the controlled adsorption of water molecules. *Small* **6**, 22, 2535 (2010)
13. W.Wang and Z.Li, Potential barrier of graphene edges. *J. Appl. Phys*, **109**, 114308 (2011)

14. J. Berashevich and T. Chakraborty, Doping graphene by adsorption of polar molecules at the oxidized zigzag edges. *Phys. Rev. B* **81**, 205431 (2010)
15. X. Lin, J. Ni and C. Fang, Adsorption capacity of H2O, NH3, CO and NO2 on the pristine graphene. *J. Appl. Phys*, **113**, 034306 (2013)
16. A.J. Pak, E. Paek and G.S. Hwang, Impact of graphene edges on enhancing the performance of electrochemical double layer capacitors. *J. Phys. Chem. C* **118**, 21770 (2014)
17. L. Wang, I. Meric, P. Y. Huang, Q. Gao, Y. Gao, H. Tran, T. Taniguchi, K. Watanabe, L. M. Campos, D. A. Muller, J. Guo, P. Kim, J. Hone, K. L. Shepard, and C. R. Dean, One-dimensional electrical contact to a two-dimensional material. *Science* **342**, 614 (2013)
18. F. Pizzocchero, L. Gammelgaard, B. S. Jessen, J. M. Caridad, L. Wang, J. Hone, P. Bøggild, and T. J. Booth, The hot-pick up technique for batch assembly of van der Waals heterostructures. *Nature Comm.* **7**, 11894 (2016)
19. P. Pedrinazzi, J.M. Caridad, D.M.A. Mackenzie, F. Pizzocchero, L. Gammelgaard, B.S. Jessen, R. Sordan, T.J. Booth and P. Bøggild. *Appl. Phys. Lett.* **112**, 033101 (2018).
20. C. Struzzi, H. Sezen, M. Amati, L. Gregoratti, M. Reckinger, J.-F. Colomer, R. Snyders, C. Bittencourt and M. Scardamaglia, Fluorine and sulfur simultaneously co-doped suspended graphene. *Appl. Surf. Sci.* **422**, 104 (2017).
21. P.G. Silvestrov and K.B. Efetov, Charge accumulation at the boundaries of a graphene strip induced by a gate voltage: Electrostatic approach. *Phys. Rev. B*, **77**, 155436-155440 (2008).
22. J.M. Caridad, S.R. Power, M.R. Lotz, A.A. Shylau, J.D. Thomsen, L. Gammelgaard, T.J. Booth, A.-P. Jauho and P. Bøggild. Conductance quantization suppression in the quantum Hall regime. *Nature Comm.* **9**, 659 (2018)
23. S. Abe, Y. Nagoya, F. Watari and H. Tachikawa. Interaction of water molecules with graphene: A density functional theory and molecular dynamics study. *Jpn. J. Appl. Phys.* **49**, 01AH07 (2010)
24. M. S. Fernández, F.M. Peeters, and N.Neek-Amal. Electric-field-induced structural changes in water confined between two graphene layers. *Phys. Rev. B*, **94**, 045436 (2016)
25. M. Klinsmann, D. Peter and H. P. Büchler, Ferroelectric quantum phase transition with cold polar molecules. *New. J. Phys,* **17**, 085002 (2015).
26. B.P. Gorshunov, V.I. Torgashev, E.S. Zhukova, V.G. Thomas, M.A. Belyanchikov, C. Kadlec, F. Kadlec, M. Savinov, T. Ostapchuk, J. Petzelt, J. Prokleska, P.V. Tomas, E.V. Pestrjakov, D.A. Fursenko, G.S. Shakurov, A.S. Prokhorov, V.S. Gorelik, L.S. Kadyrov, V.V. Uskov, R.K. Keremer and M. Dressel, Incipient ferroelectricity of water molecules confined to nano-channels of beryl. *Nature Comm.* **7**, 12842 (2016).

27. D.J. Griffiths. Introduction to electrodynamics. *Prentice Hall* (1999)
28. L. Gammelgaard, J.M. Caridad, A. Cagliani, D.M.A. Mackenzie, D.H. Petersen, T.J. Booth and P. Bøggild, Graphene transport properties upon exposure to PMMA processing and heat treatments. *2D Materials*, **1**, 035005 (2014).
29. F. Guinea ad N.R. Walet. Interaction between point charges, dipoles and graphene layers. https://arxiv.org/abs/1605.08429
30. P. Simonet, D. Bischoff, A. Moser, T. Ihn and K. Ensslin, Graphene nanoribbons: relevance of etching process. *J.Appl. Phys.* **117**, 184303-184307 (2015).
31. M. Baraket, S.G. Walton, E.H. Lock, J.T. Robinson and F.K. Perkins, The functionalization of graphene using electron-beam generated plasmas. *Appl. Phys. Lett.* **96**, 231501 (2010).
32. K-I. Ho, C-H. Huang, J-H. Liao, W. Zhang, L-J. Li, C-S. Lai and C-Y. Su, Fluorinated graphene as high performance dielectric materials and the applications for graphene nanoelectronics. *Sci. Rep.* **4**, 5893 (2014).
33. D.M.A. Mackenzie, J.D. Buron, P.R. Whelan, J.M. Caridad, M. Bjergfelt, B. Luo, A. Shivayogimath, A.L. Smitshuysen, J.D. Thomsen, T.J. Booth, L. Gammelgaard, J. Zultak, B.S. Jessen, P. Bøggild and D.H. Petersen. Quality assessment of graphene: Continuity, uniformity and accuracy of mobility measurements. *Nano Research*, **10**, 3596 (2017)
34. J.P. Perdew and A. Zunger, Self-interaction correction to density-functional approximations for many-electron systems. *Phys. Rev. B* **23**, 5048 (1981).
35. T. Gunst, K. Kaasbjerg and M. Brandbyge, Flexural-Phonon Scattering Induced by Electrostatic Gating in Graphene. *Phys. Rev. Lett.* **118,** 046601 (2017)

Acknowledgments

We acknowledge stimulating discussions with A. Cagliani, M. Scardamaglia and L. Camilli.
Funding: This work was supported by the Danish National Research Foundation Center for Nanostructured Graphene, project DNRF103, the EU Seventh Framework Programme (FP7/2007-2013) under grant agreement number FP7-6040007 'GLADIATOR' and the EC Graphene FET Flagship, grant agreement number 604391. J.M.C. acknowledges funding from the Otto Mønsteds Fund. J. E. S. acknowledges support by the European Structural and Investment Funds in the FEDER

component, through the Operational Competitiveness and Internationalization Program (COMPETE 2020) [Project nº 002797; Funding Reference: POCI-01-0247-FEDER-002797] .

Author contributions: J.M.C. conceived the idea and interpreted the data. J.M.C, and P.P. fabricated the devices and measured their electrical properties. G.C., A.I., T.G. and M.B. undertook the DFT simulations. J.M.C and J.E.S. carried out the electrostatic calculation. M.B. developed the mean-field model. J.E.S. performed the statistical mechanics calculation. J.M.C, G.C., T.G., J.E.S and M.B. carried out the data analysis. J.M.C., M.B., and P.B. wrote the manuscript, with comments from all authors.

Competing interests: The authors declare no financial interests.

Supporting information: (1) discussion of the measured effect in comparison with conventional charge hysteresis, (2) Analysis of electrical field at the graphene edges, (3) atomistic calculations of binding energies of the adsorbed molecules, (4) Symmetric positioning of different polar molecules at graphene edges, (5) DFT calculations on armchair edges, (6) calculations regarding the molecular occupation at the edges, (7) Electrostatic calculations of total charge in devices due to oriented dipoles, and (8) model for the molecular switching

Data and materials availability: All the data needed to evaluate the conclusions in the paper are present in the paper and/or the Supplementary Materials. Additional data related to this paper may be requested from the authors.

Figures

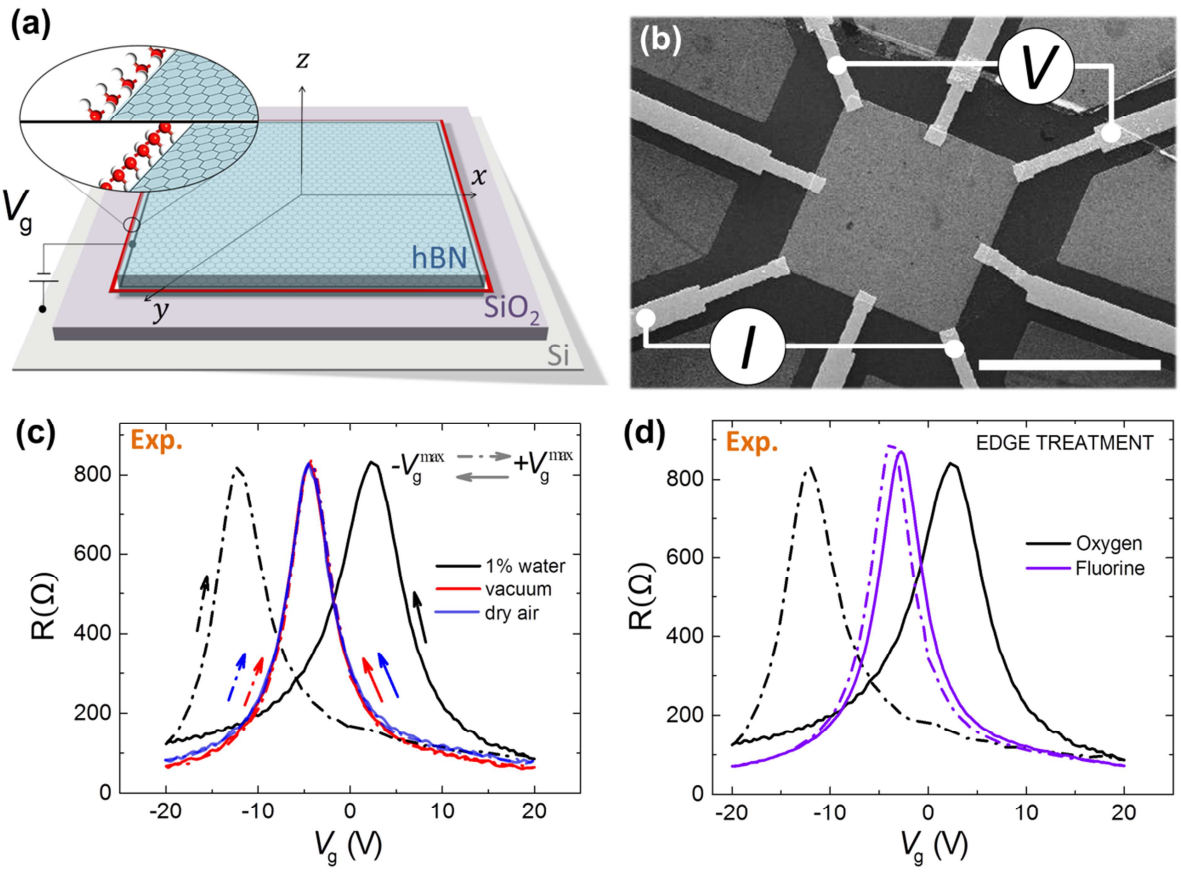

Figure 1. Polar molecules at graphene edges in micrometer-scaled gated devices. (a), Schematic of the squared graphene device encapsulated by hBN with water molecules at edges. Inset shows the two collectively aligned molecular configurations at graphene edges: above and below the graphene plane. (b), Scanning electron micrograph (SEM) of one of our devices. Scale bar is 5µm. (c), Resistance $R = V / I$ measured across one of our devices (Device 1) immersed in three different environments: vacuum (red), dry air (blue), and dry air with 1% water vapour (black). The resistance is measured following two sweep sequences: $+V_g^{max} \rightarrow -V_g^{max}$ (continuous line) and $-V_g^{max} \rightarrow +V_g^{max}$ (dashed lines). (d), Resistance $R = V / I$ measured across a device (Device 1) after fluorine (violet) and oxygen (black) edge treatments in an environment composed of dry air with 1% water vapour.

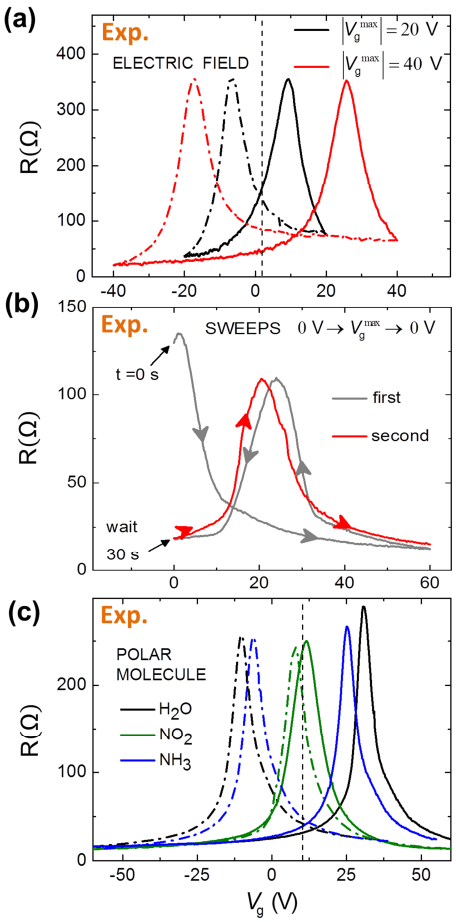

Figure 2. Electrical measurements of micrometer-size gated graphene devices in different conditions. (a) R measured across one of our devices (Device 2) with oxygen edge-treatment immersed in dry air with 1% water vapour following two sweep sequences: $+V_g^{max} \rightarrow -V_g^{max}$ (continuous line) and $-V_g^{max} \rightarrow +V_g^{max}$ (dashed-dot lines). Here we take two values for $|V_g^{max}|$: 20V (black) and 40V (red). (b), Change of charge neutrality point in one of our devices (Device 3) when sweeping V_g following the sequence $0 \rightarrow V_g^{max} \rightarrow 0$ two consecutive times. During the first sweep, the charge neutrality point has changed from V_{CNP}^{0}~0.5V to $V_{CNP}^{(z>0)}$ ~ 20V, indicative of molecular polarization. After waiting 30 seconds at V_g=0V a second sweep $0 \rightarrow V_g^{max}$ was undertaken. The charge neutrality point had clearly remained at the position $V_{CNP}^{(z>0)}$, this is, molecules remain polarized (albeit a small shift due to depolarization effects occurring at room temperature). (c), R measured across one of our devices (Device 4) with oxygen edge-treatment immersed in dry air with 1% water vapour (black) , dry air with 1% nitrogen dioxide (green) and dry air with 1% ammonia (blue).

Vertical dashed lines in panels (a) and (c) indicate the position of the charge neutrality point when devices are measured in vacuum.

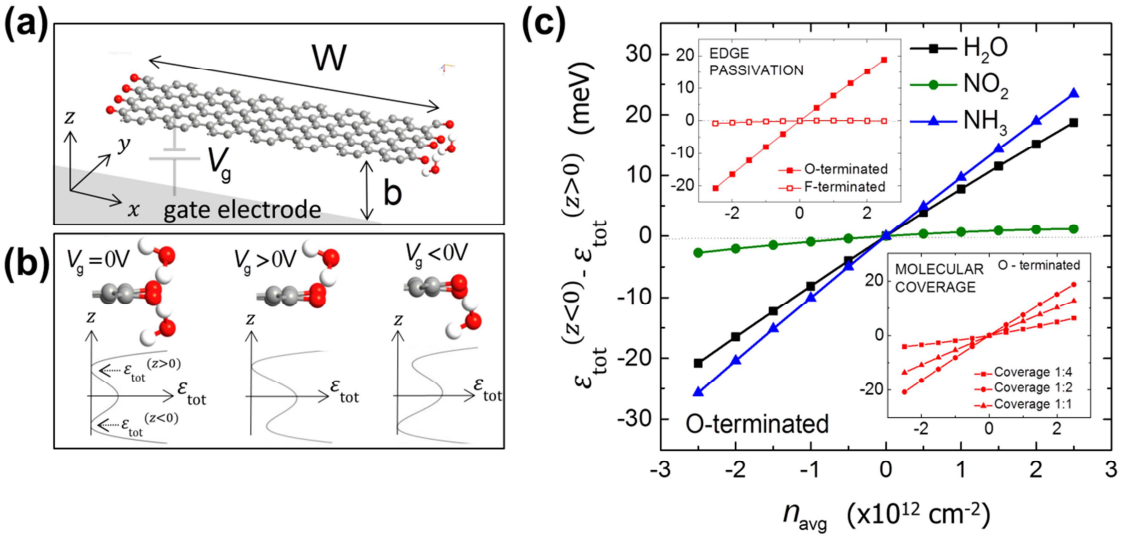

Figure 3. Atomistic DFT calculations of gated nanoribbons with edge adsorption. (a), Simulated graphene ribbon (periodic in the y direction) of width W (3, 13 and 23 nm) with a gate electrode underneath. (b), Two stable configurations ("above" and "below" the graphene plane w.r.t the gate) of water molecules at graphene edges (passivated with oxygen) and preferential placement depending on V_g. Graphs below show an schematic of the total energy ε_{tot} (represented as a double well with two minimum positions below $\varepsilon_{tot}^{(z<0)}$ and above $\varepsilon_{tot}^{(z>0)}$ the graphene plane w.r.t the gate electrode) and its evolution with V_g. (c), Energy difference between the two minimums (stable molecular position), at different averaged carrier densities n_{avg} for three different types of polar molecule: water (H_2O), nitrogen dioxide (NO_2) and ammonia (NH_3). $\varepsilon_{tot}^{(z<0)} - \varepsilon_{tot}^{(z>0)}$ shows additional dependencies on edge termination (upper inset, simulation done with H_2O), type of polar molecule at the edge and occupation (lower inset, simulation done with H_2O).

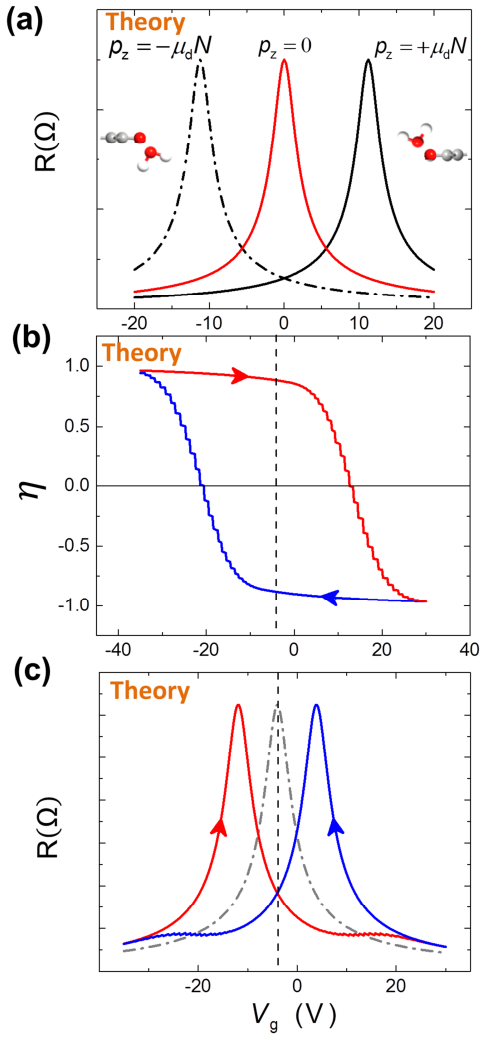

Figure 4. Ferroelectricity of polar molecules at the edges of micron-size graphene devices. (a) Electrostatic model, showing the calculated resistance in the device for different net dipole moments along the graphene edge: molecules above the graphene plane ($p_z = +\mu_d N$), crown of molecules below the graphene plane ($p_z = -\mu_d N$) and absence of the crown of dipoles ($p_z = 0$) . A net dipole along a graphene edge introduces considerably ambipolar doping (shift in V_{CNP}) in a micrometer size graphene device, symmetric for the two opposite molecular orientations. (b), Calculated transcendental equation $\eta = \tanh(K\eta + b)$, showing hysteretic behaviour for cyclic gate-sweeps. (c), Calculated resistance $R(V_g, p_z)$, including η obtained in (a), reflecting the observed hysteretic behavior in our experiments (Figure 1(c)). In panels b-c, V_{CNP}^0 of our experimental device is indicated by verticals dashed lines.

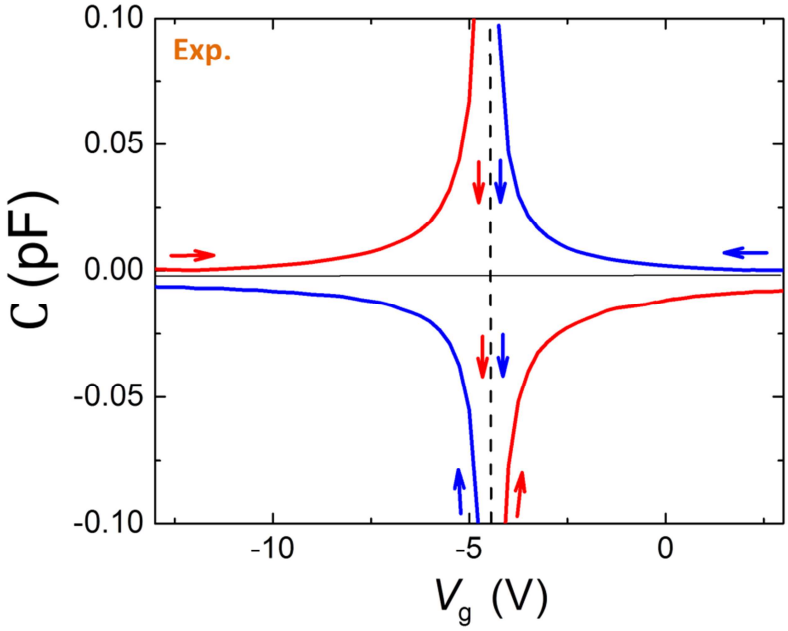

Figure 5. Memcapacitive behaviour in graphene based transistors with polar molecules at edges for symmetric sweeps of V_g **.** Extracted ambipolar, hysteretic and diverging capacitance in one of our devices (Figure (c)). This capacitance exhibits a typical behaviour of polarizable memcapacitive systems *(6)*. V_{CNP}^{0} is indicated by verticals dashed lines.